

# Performance of a Kinetic Inductance Traveling-Wave Parametric Amplifier at 4 Kelvin: Toward an Alternative to Semiconductor Amplifiers

M. Malnou<sup>1,2,\*</sup>, J. Aumentado,<sup>1</sup> M.R. Vissers,<sup>1</sup> J.D. Wheeler,<sup>1</sup> J. Hubmayr<sup>1</sup>,<sup>1</sup> J.N. Ullom,<sup>1,2</sup> and J. Gao<sup>1,2</sup>

<sup>1</sup>*National Institute of Standards and Technology, Boulder, Colorado 80305, USA*

<sup>2</sup>*Department of Physics, University of Colorado, Boulder, Colorado 80309, USA*

(Received 15 October 2021; revised 7 February 2022; accepted 14 March 2022; published 5 April 2022)

Most microwave readout architectures in quantum computing or sensing rely on a semiconductor amplifier at 4 K, typically a high-electron mobility transistor (HEMT). Despite its remarkable noise performance, a conventional HEMT dissipates several milliwatts of power, posing a practical challenge to scale up the number of qubits or sensors addressed in these architectures. As an alternative, we present an amplification chain consisting of a kinetic inductance traveling-wave parametric amplifier (KITWPA) placed at 4 K, followed by a HEMT placed at 70 K, and demonstrate a chain-added noise  $T_{\Sigma} = 6.3 \pm 0.5$  K between 3.5 and 5.5 GHz. While, in principle, any parametric amplifier can be quantum limited even at 4 K, in practice we find the performance of the KITWPA to be limited by the temperature of its inputs and by an excess of noise  $T_{\text{ex}} = 1.9$  K. The dissipation of the rf pump of the KITWPA constitutes the main power load at 4 K and is about 1% that of a HEMT. These combined noise and power dissipation values pave the way for the use of the KITWPA as a replacement for semiconductor amplifiers.

DOI: 10.1103/PhysRevApplied.17.044009

## I. INTRODUCTION

Superconducting parametric amplifiers have been studied and refined for decades [1–8], yet they have always been used in the same configuration: as preamplifiers placed at millikelvin temperatures, followed by a 4-K stage low-noise amplifier, conventionally a high-electron mobility transistor (HEMT). While Al-based parametric amplifiers can only operate well below the critical temperature of aluminum ( $T_c \sim 1.2$  K), Nb-based Josephson amplifiers ( $T_c \sim 9$  K) [2,5,9] or Nb-Ti-N-based kinetic amplifiers ( $T_c \sim 14$  K) [4,8,10–12] can operate at much higher temperatures, in particular at 4 K.

At 4 K, HEMTs are commercially available and typically achieve input noise temperatures of just a few kelvins, with bandwidths spanning several gigahertz. They are integral to superconducting quantum computer architectures [13], to dark-matter searches [14–16], and to the readout of superconducting transition-edge sensors or microwave kinetic inductance detectors [17,18]. However, cryogenic HEMTs require several milliwatts of power and the dissipated heat load can quickly become a serious challenge when designing experiments that require scaling to massive detector or qubit channel counts. For example, in both the Lynx [19,20] and the Origin Space Telescope [21–23], two of the four large mission concepts

for observatories presented in the 2020 Astronomy and Astrophysics Decadal Survey [24], about ten HEMTs are planned to measure signals from roughly 10 000 readout channels and the power dissipation from the HEMTs is the single largest power load on the 4-K stage of the instrument. In space, achieving 10 mW of cooling power at 4 K is extremely challenging; therefore, techniques for measuring gigahertz signals that can reduce this heat load are of great interest.

At millikelvin temperatures, the Nb-Ti-N-based kinetic inductance traveling-wave parametric amplifier (KITWPA) has shown promising performance [4,8,10,11,25,26]. In particular, its gigahertz bandwidth along with its nanowatt input saturation power makes it compatible with high-channel-count applications and it can operate close to the quantum limit [8,25]. Furthermore, Nb-Ti-N resonators have internal quality factors  $Q \gtrsim 10^3$  at 4 K due to their high  $T_c$  [27], so the KITWPA chip should be almost dissipationless. In addition, the three-wave mixing (3WM) mode of operation has reduced its pump power requirements to the few microwatts range [8,28], suggesting that the power dissipation at 4 K can be made much smaller than that generated by common HEMTs.

In this paper, we ask: can a KITWPA replace a conventional 4-K stage semiconductor amplifier? Although one might expect parametric gain at 4 K, can one also expect it to retain its noise performance at such high temperature? Here we show that, in principle, a “hot” parametric

\* maxime.malnou@nist.gov

amplifier can be quantum limited, as long as its input fields are well thermalized to a cold bath. Using a shot-noise tunnel junction (SNTJ), we measure the total chain-added noise of an amplification chain configured with the KITWPA at 4 K, followed by a HEMT placed at 70 K, and find  $T_{\Sigma} = 6.3 \pm 0.5$  K between 3.5 and 5.5 GHz. This noise level is comparable to that of a well-optimized chain with a single HEMT placed at 4 K. Accounting for the contribution of each stage in the amplification chain, we estimate that the KITWPA alone generates  $1.9 \pm 0.2$  K of excess noise, on par with the noise added by most commercial HEMTs [29]. Meanwhile, the power load at 4 K, predominantly due to dissipating the rf pump, is currently about  $100 \mu\text{W}$ , or 1% of that of a HEMT. Together, these measurements pave the way toward a more power-efficient and lower-noise alternative to semiconductor amplifiers at 4 K.

## II. THEORY AND EXPERIMENTAL PRINCIPLE

The fundamental limit on the noise added by a lossless phase-insensitive parametric amplifier is often described as originating from an internal mode [30–32]. But this mode is not an inaccessible internal degree of freedom. Rather, it refers to the input “idler” mode and therefore this ideal amplifier should properly be described as a four-port device: two inputs and two outputs, at the signal and idler frequencies (the idler output is usually not monitored). In this context, the mean amplifier output signal power is, in units of photons [8],

$$N_{\text{out}}^s = GN_{\text{in}}^s + (G - 1)N_{\text{in}}^i, \quad (1)$$

where  $G$  is the amplifier signal power gain and  $N_{\text{in}}^s$  ( $N_{\text{in}}^i$ ) is the input power at the signal (idler) frequency. Here, regardless of its physical temperature, the quantum-limited nature of the amplifier only depends on the input idler state: when it is vacuum  $N_{\text{in}}^i = 1/2$ , in the high-gain limit the amplifier adds half a photon worth of noise energy to the input-referred signal  $N_{\text{in}}^s$ .

To test whether a “hot” parametric amplifier can remain quantum limited, we design the amplification chain illustrated in Fig. 1, where a KITWPA is placed at 4 K but its signal and idler inputs are connected to the millikelvin stage. Then, provided that (i) the gain of the KITWPA is enough to overcome the following loss and amplifier-added noise, (ii) the inputs of the KITWPA are cold, and (iii) the KITWPA is lossless, i.e., does not add any excess of noise on top of that from its inputs, the noise added by the entire chain should reach the quantum limit (half a photon) (see Appendix A 1).

Operating the KITWPA in a 3WM fashion [8,26], we employ a bias tee (BT) and a directional coupler (DC) to deliver, respectively, a dc current and an rf pump to its physical input port. Both the BT and the DC are placed

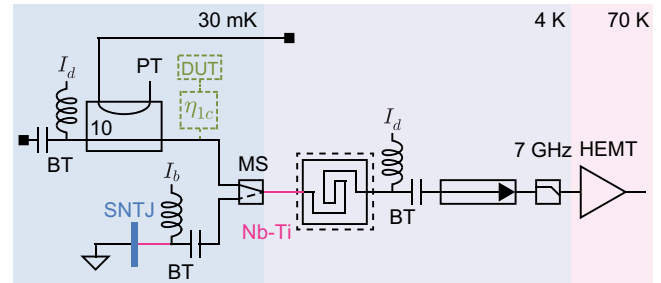


FIG. 1. A schematic of the amplification chain. The KITWPA (squared spiral) is magnetically shielded (dashed square) and placed at 4 K while the HEMT operates at 70 K, protected from the strong KITWPA pump tone (PT) by a low-pass filter. The PT then dissipates into the isolator (4–12 GHz). When the microwave switch (MS) is in its top position, the PT is delivered to the KITWPA via a directional coupler (DC), whereas two bias tees (BTs) allow the dc current  $I_d$  to flow in and out of the chain, through the KITWPA. A hypothetical device under test (DUT) is coupled to the chain with efficiency  $\eta_{1c}$ . When the MS is in its bottom position, the SNTJ delivers a known noise [33] to the input of the chain, the power of which depends on the current  $I_b$  (delivered via a BT) with which the SNTJ is biased.

at 30 mK, behind a hypothetical device under test (DUT) coupled to the readout line, thereby minimizing insertion loss between the DUT and the KITWPA. This configuration is particularly suitable when the DUT represents an array of resonators, such as microwave kinetic inductance detectors [25,34] or a microwave superconducting quantum interference device multiplexer [35,36].

To measure the added noise of such a chain, we insert a microwave switch (MS) that allows us to alternate between the KITWPA biasing components and a calibrated noise source, consisting of a SNTJ [8,37]. We first obtain the added noise  $N'_{\Sigma}$  of the chain when the MS is toggled toward the SNTJ (see Appendix E 1). Then, after actuating the MS, we turn on the KITWPA and measure the level  $r$  to which the output noise rises. We then deduce the chain-added noise  $N_{\Sigma}$  using

$$\frac{r}{G} = \frac{N_{\Sigma} + N_c}{N'_{\Sigma} + N_c}, \quad (2)$$

where  $G$  is the KITWPA gain and  $N_c$  is the vacuum noise (see Appendix A 2).

## III. PERFORMANCE AT 4 K

The results of such a measurement are presented in Fig. 2, performed when using a commercial HEMT and a KITWPA, the design and millikelvin performance of which have been described elsewhere [8]. With the MS actuated toward the DC and BT, we operate the KITWPA at various gains, from an average of 2.5 dB to 18 dB between 3.5 and 5.5 GHz [see Fig. 2(a)]; the higher gain

profile remains flat, with less-than-3-dB ripples in that band. For each operating gain  $G$ , we record the noise rise  $r$  on a spectrum analyzer (SA) and form  $T_\Sigma = N_\Sigma \hbar\omega/k_B$  (where  $\hbar$  is the reduced Planck constant and  $k_B$  is the Boltzmann constant) using Eq. (2). In Fig. 2(b), we show  $T_\Sigma$  as a function of the frequency, when the KITWPA is operated at low and high gain (gray and black curves, respectively), along with  $T'_\Sigma = N'_\Sigma \hbar\omega/k_B$ , obtained when the MS is actuated toward the SNTJ (purple curve). At high gain,  $T_\Sigma = 6.3 \pm 0.5$  K between 3.5 and 5.5 GHz (with uncertainty dominated by that of the output power of the chain, known within  $\pm 0.3$  dB). To our knowledge, it is the first time that such a low and broadband noise performance has been obtained without the use of a semiconductor amplifier at 4 K.

As discussed in Sec. II, three possible sources of noise prevent  $T_\Sigma$  from reaching the quantum limit: (i) insufficient KITWPA gain, (ii) warm KITWPA inputs, and (iii) KITWPA excess noise. Although, from a user perspective, only  $T_\Sigma$  matters, knowledge of the separate contribution of these sources is interesting from an amplifier-design perspective, because it indicates if and how  $T_\Sigma$  may be improved. In Fig. 2(c), we present the variation of  $T_\Sigma$  as a function of  $G$ , at two different frequencies. As  $G$  increases,  $T_\Sigma$  reaches an asymptotic lower bound. Therefore, the high-gain regime of our KITWPA is enough to overcome the following loss and HEMT-added noise; operating at higher gain would not improve the chain-added noise.

To evaluate the noise coming from the KITWPA inputs, we separately measure at 4 K the transmission

efficiencies of each stage in the amplification chain (see Appendix F). Each efficiency acts as an effective noise source, the temperature of which is governed by a beam-splitter interaction (see Appendix A 1). In Table I we report the transmission efficiencies and corresponding noise temperatures of the various stages, either when considered separately (intrinsic noise) or within the amplification chain (chain-input-referred noise). Clearly, the temperature of the KITWPA inputs is dominated by the effect of  $\eta_{1h} = 0.8$ , the transmission efficiency at 4 K between the DUT and the KITWPA. It generates 2.1 K of noise at the input of the amplifier (and 2.6 K when referred to the input of the chain). Practically,  $T_\Sigma$  may be significantly decreased with increasing  $\eta_{1h}$ : for example, with  $\eta_{1h} = 0.9$ ,  $T_\Sigma$  would drop from 6.3 K to 4.5 K. We believe this performance to be achievable, because most of our warm-insertion loss originates in the KITWPA packaging, the printed circuit boards and connectors of which may be made less dissipative.

Subtracting the (input-referred) noise generated by all the inefficient transmissions from  $T_\Sigma$ , we deduce the KITWPA excess noise: at the input of the chain, it amounts to 2.9 K, equivalent to an intrinsic excess noise temperature  $T_{ex} = 1.9 \pm 0.2$  K, on par with that of the HEMT at 4 K [29]. This noise is associated with some internal loss (see Appendix B).

As a fair comparison to  $T_\Sigma$ , we measure the noise temperature  $T_{\Sigma 2}$  added by a well-optimized chain, employing only a HEMT at 4 K (see Appendix D). Between 3.5 and 5.5 GHz,  $T_{\Sigma 2} = 3.5 \pm 0.3$  K (with uncertainty

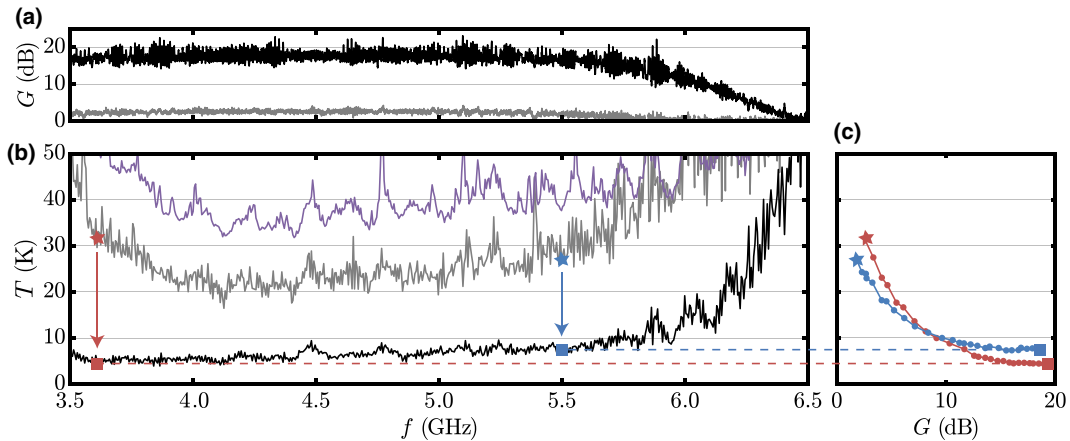


FIG. 2. Chain-added noise measurement. (a) The KITWPA gain  $G$  (ratio pump on or off) as a function of the frequency (measured with a vector network analyzer) is shown for two rf pump powers ( $P_p$ ): at low pump power (gray curve,  $P_p = -37$  dBm at the input of the KITWPA) and high pump power (black curve,  $P_p = -29$  dBm). In both cases, the pump frequency is  $f_p = 8.979$  GHz and the KITWPA is dc biased with  $I_d = 0.7$  mA. (b) We first measure the frequency-dependent chain-added noise  $T'_\Sigma$  (purple curve) with the SNTJ. Below 4 GHz and above 6 GHz,  $T'_\Sigma$  increases because we reach the pass-band edge of the components in the amplification chain (HEMT, isolator, and low-pass filter). Then, we deduce the chain-added noise  $T_\Sigma$  when the KITWPA operates at the low (gray curve) and high (black curve) gain  $G$  presented in (a). The points at two witness frequencies (3.6 GHz and 5.5 GHz) underline how the noise diminishes (from stars to squares) when the gain increases. (c) At these two frequencies, the variation of  $T_\Sigma$  as a function of the gain shows that the lowest noise temperature (square) reaches an asymptote.

TABLE I. The noise contribution of each stage of the amplification chain, averaged between 3.5 and 5.5 GHz. The DUT signals are routed to the signal input of the amplifier with efficiency  $\eta_{1c}$  at 30 mK (i.e., there is  $-10 \log(\eta_{1c})$  dB of insertion loss) and with efficiency  $\eta_{1h}$  at 4 K. After the KITWPA, signals are routed with efficiency  $\eta_2$  to the HEMT input (see Appendix A 1). From the transmission efficiencies, we calculate the intrinsic and chain-input-referred noise temperatures, using the expressions reported in Table III. Note that for the noises related to  $\eta_{1c}$  and  $\eta_{1h}$ , the contribution of the signal and idler paths are added. The intrinsic HEMT-added noise at 70 K (first stage of our dilution refrigerator)  $T_H = 13.4 \pm 0.4$  K lies between the HEMT-added noise at 4 K and that at 296 K [29].

Sources of noise	$\eta_{1c}$	$\eta_{1h}$	$G$	$\eta_2$	$G_H$
Transmission efficiency	0.80	0.80	—	0.51	—
Insertion loss (dB)	1	1	—	2.9	—
Intrinsic noise (K)	0.16	2.1	1.9	3.9	10.7
Input-referred noise (K)	0.16	2.6	2.9	0.1	0.6

here dominated by that of the SNTJ impedance,  $48.2 \pm 3.5 \Omega$ ). Therefore, while not surpassing it, the KITWPA-based solution approaches the HEMT-based performance.

#### IV. POWER CONSUMPTION

In combination with having a competitive amplification and noise performance compared to that of a HEMT, the 4-K stage KITWPA is expected to consume much less power. In fact, it typically requires an rf pump power  $P_p \sim -30$  dBm (i.e.,  $1 \mu\text{W}$ ), several orders of magnitude lower than the power requirement for a standard (approximately 10 mW [29]) or even state-of-the-art ( $300 \mu\text{W}$  [38]) HEMT. Note, however, that  $P_p$  does not account for the dissipation along the pump line. In our current setup, the pump travels to the KITWPA via a 10-dB attenuator at 4 K and through the weakly coupled port of a 10-dB DC at the millikelvin stage (see Appendix C 1). Therefore, in our experiment, a typical  $-30$ -dBm pump tone delivered to the KITWPA translates into dissipating  $99 \mu\text{W}$  at 4 K (the DC being terminated at 4 K). But such a heavy attenuation is not mandatory: in principle, the high-pass filter (HPF) we employ at the millikelvin stage suffices to prevent the room-temperature 300-K noise from directly contaminating the signal and idler bands. At the pump frequency, this noise is negligible compared with the power of the tone and therefore does not affect the dynamics of the KITWPA (in the limit of nondiverging gain [12]). So instead of being

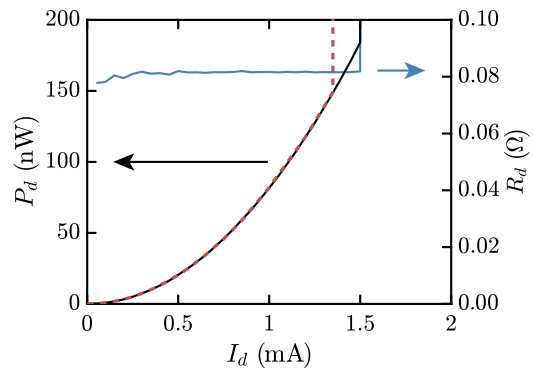


FIG. 3. The characterization of the KITWPA dc power dissipation. The dissipated power  $P_d$  (left-hand  $y$  axis) is shown as a function of the bias current  $I_d$  for two situations: when the pump of the KITWPA is off (solid black line) and when  $P_p = -20$  dBm (dashed red line). In the pump-off situation, the resistance  $R_d$  (right-hand  $y$  axis) is also shown as a function of  $I_d$  (blue curve).

injected through the 4-K stage attenuator and millikelvin-stage DC, the pump could simply pass through the HPF and enter the rf port of the input bias tee. Furthermore, at 4 K,  $P_p$  is currently dissipated in the isolator placed before the HEMT, which could also be avoided by using a diplexer to redirect the pump to higher temperature. With these strategies, the dissipation associated with the pump can be reduced below  $1 \mu\text{W}$  at 4 K. Further possible improvements of the amplification chain—in particular, targeted for qubit readout applications—are discussed in Appendix C 2.

However, the KITWPA also requires a non-negligible dc bias  $I_d \sim 1$  mA, which may dissipate and generate heat. We measure the corresponding dissipated power  $P_d$  with a four-point probe setup (see Appendix G): reading the voltage drop  $V_d$  across the KITWPA, we then retrieve  $P_d = V_d I_d$ . In Fig. 3, we show  $P_d$  as function of  $I_d$ , when the rf pump is off (solid black line) or, instead, very strong ( $P_p = -20$  dBm, dashed black line). In both cases, at  $I_d = 1$  mA we obtain  $P_d \simeq 100$  nW, several orders of magnitude lower than what a HEMT consumes. We also show the resistance  $R_d = V_d / I_d$  (right-hand  $y$  axis) as a function of  $I_d$ . Under normal operation, i.e., for  $I_d < 1.5$  mA, the resistance across the four-point probes (encompassing the KITWPA, its packaging, and the BT at 4 K) is  $R_d = 80$  m $\Omega$ . Conversely,  $R_d$  increases sharply to approximately  $\sim 1$  k $\Omega$  when  $I_d > 1.5$  mA, because superconductivity breaks down inside the KITWPA, probably at a weak link [8,39]. Note that the transition to this dissipative regime happens at slightly reduced  $I_d$  when  $P_p = -20$  dBm, suggesting that both the dc and the rf currents can activate the weak link. Voltage biasing the KITWPA with a small (approximately 100- $\Omega$ ) shunting resistor would alleviate transitioning to this regime.

## V. CONCLUSION

Despite their remarkable noise performance at 4 K, semiconductor amplifiers remain power hungry. This dissipation may limit the scale of future applications, for which large arrays ( $> 10^5$ ) of detectors or qubits would require tens to hundreds of low-noise amplifiers. As an alternative, we investigate the use of a parametric amplifier at 4 K: the KITWPA. Using a SNTJ as a calibrated noise source, we measure the noise added by an amplification chain where the KITWPA is the sole 4-K stage amplifier. In principle, this chain can remain quantum limited; in practice, when the KITWPA is operated at an average gain of 18 dB within a 2-GHz bandwidth (and with less-than-3-dB gain ripples in that band) we measure an average chain-added noise of  $6.3 \pm 0.5$  K, comparable to that of a chain where the HEMT is the 4-K stage amplifier. This performance is limited mostly by the insertion loss at 4 K preceding the KITWPA and by an excess of noise  $T_{\text{ex}} = 1.9 \pm 0.2$  K. Furthermore, the heat load at 4 K, currently in the  $100\text{-}\mu\text{W}$  range, is due to dissipating the rf pump. It is 2 orders of magnitude lower than what a conventional HEMT generates and can straightforwardly be reduced below 1  $\mu\text{W}$ . This work is a successful implementation of a broadband, high-gain, low noise, and power-efficient microwave parametric amplifier at 4 K. As such, it may constitute a shift in the readout architecture for large numbers of microwave resonators.

## ACKNOWLEDGMENTS

Certain commercial materials and equipment are identified in this paper to foster understanding. Such identification does not imply recommendation or endorsement by the National Institute of Standards and Technology (NIST); nor does it imply that the materials or equipment identified are necessarily the best available for the purpose. We gratefully acknowledge support from the NIST Program on Scalable Superconducting Computing, the National Aeronautics and Space Administration (NASA) under Grant No. NNH18ZDA001N-APRA, and the Department of Energy (DOE) Accelerator and Detector Research Program under Grant No. 89243020SSC000058.

## APPENDIX A: ADDED NOISE

### 1. Chain-added noise

Figures 4(a) and 4(b) recast the amplification chain presented in Fig. 1 in a diagram of cascaded transmission efficiencies and gains, when the MS is activated toward the KITWPA biasing components [Fig. 4(a)] or toward the SNTJ [Fig. 4(b)]. Considering the situation in Fig. 4(a) first, a signal with photon number  $N_{\text{in}}^s$  at the input of the chain (that would be generated by the hypothetical DUT), undergoes amplification and loss when propagating to the

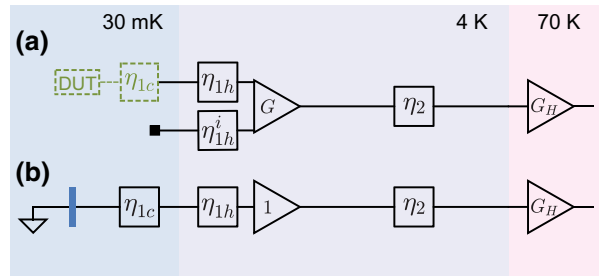


FIG. 4. A diagram of the cascaded transmission efficiencies and gains, when the MS is activated (a) toward the KITWPA biasing components or (b) toward the SNTJ.

chain:

$$N_{1c}^s = \eta_{1c} \left( N_{\text{in}}^s + \frac{1 - \eta_{1c}}{\eta_{1c}} N_c \right), \quad (\text{A1})$$

$$N_{1h}^s = \eta_{1h} \left( N_{1c}^s + \frac{1 - \eta_{1h}}{\eta_{1h}} N_h \right), \quad (\text{A2})$$

$$N_{1h}^i = \eta_{1h}^i \left( N_c + \frac{1 - \eta_{1h}^i}{\eta_{1h}^i} N_h \right), \quad (\text{A3})$$

$$N_2^s = G(N_{1h}^s + N_{\text{ex}}^s) + (G - 1)(N_{1h}^i + N_{\text{ex}}^i), \quad (\text{A4})$$

$$N_3^s = \eta_2 \left( N_2^s + \frac{1 - \eta_2}{\eta_2} N_h \right), \quad (\text{A5})$$

$$N_4^s = G_H(N_3^s + N_H), \quad (\text{A6})$$

where the variables are all defined in Table II.

Assuming that the HEMT gain is sufficient to overcome any following loss and amplifier-added noise, the power at the signal frequency reaching the SA is directly proportional to  $N_4^s$ . Using Eqs. (A1) to (A6), and in the simpler case where  $G \gg 1$  and where the idler and signal transmission efficiencies at 4 K are equal,  $\eta_{1h}^i = \eta_{1h}$ , we have

$$N_4^s = G_H \eta_2 G \eta_{1h} \eta_{1c} (N_{\text{in}}^s + N_{\Sigma}), \quad (\text{A7})$$

where

$$\begin{aligned} N_{\Sigma} = & \frac{2 - \eta_{1c}}{\eta_{1c}} N_c + 2 \frac{1 - \eta_{1h}}{\eta_{1h} \eta_{1c}} N_h + \frac{1}{\eta_{1h} \eta_{1c}} N_{\text{ex}} \\ & + \frac{1 - \eta_2}{\eta_2 G \eta_{1h} \eta_{1c}} N_h + \frac{1}{\eta_2 G \eta_{1h} \eta_{1c}} N_H \end{aligned} \quad (\text{A8})$$

is the chain-added noise. The first line on the right-hand side of Eq. (A8) can be identified as the KITWPA added noise; it depends not only on the KITWPA excess noise  $N_{\text{ex}} = N_{\text{ex}}^s + N_{\text{ex}}^i$  but also on the cold and warm transmission efficiencies between the KITWPA and the input of

the chain. The second line represents the contributions of the elements placed after the KITWPA: the transmission efficiency  $\eta_2$  (first term) and the HEMT-added noise (second term); they are damped at sufficiently high gain  $G$ . In the high-gain limit, with perfect transmission efficiencies  $\eta_{1c} = \eta_{1h} = 1$  (i.e., the inputs of the KITWPA are perfectly thermalized to the cold bath) and without excess noise ( $N_{ex} = 0$ ), we verify that  $N_\Sigma = 1/2$ , the minimum chain-added noise.

All the terms in Eq. (A8) are referred to the input of the chain: the noise from each source is divided by the transmission efficiencies and gain preceding it. Conversely, the noise intrinsic to each stage is chain independent. The expressions for the chain-input-referred and intrinsic noise for each stage are reported in Table III.

To calculate  $N'_\Sigma$  (the chain-added noise when the KITWPA is off and the MS is actuated toward the SNTJ), we propagate the SNTJ calibrated noise  $N_{in}^s$  (which is our “signal”) through the chain shown in Fig. 4(b). Here,  $\eta_{1c}$  accounts for the cold loss coming, in particular, from the SNTJ packaging and from the following BT. Meanwhile, the unpumped KITWPA acts as a passive element of gain 1; therefore, we need not keep track of the noise entering the idler port [8,40], because the KITWPA output signal does not contain the idler component, as can be seen from Eq. (1). We thus obtain the HEMT-output signal power,

$$N_4^{s'} = G_H \eta_2 \eta_{1h} \eta_{1c} (N_{in}^s + N'_\Sigma), \quad (\text{A9})$$

TABLE II. A list of the variables pertaining to the amplification chain [see Figs. 1(b) and 1(c)]. The variables designating a power (termed using  $N$ ) are in units of quanta. The transmission efficiencies are dimensionless and the gains are linear.

Variable name	Definition
$N_{in}^s$	Input signal of the chain
$N_c$	Vacuum noise
$N_{1c}^s$	Cold stage output signal
$N_h$	4-K stage thermal noise
$N_{1h}^s$	KITWPA input signal
$N_{1h}^i$	KITWPA input idler
$N_{ex}^s$	Signal-to-signal path KITWPA excess noise
$N_{ex}^i$	Idler-to-signal path KITWPA excess noise
$N_{ex}$	Overall KITWPA excess noise
$N_H$	HEMT-added noise
$N_2^s$	KITWPA output signal
$N_3^s$	HEMT input signal
$N_4^s$	HEMT output signal
$\eta_{1c}$	Cold-stage signal transmission efficiency
$\eta_{1h}$	4-K stage signal transmission efficiency
$\eta_{1h}^i$	4-K stage idler transmission efficiency
$\eta_2$	KITWPA-to-HEMT transmission efficiency
$G$	KITWPA signal power gain
$G_H$	HEMT signal power gain

TABLE III. The noise generated by each stage in the amplification chain.

Sources of noise	Chain-input-referred noise	Intrinsic noise
$\square \eta_{1c}$	$\frac{2-\eta_{1c}}{\eta_{1c}} N_c$	$\frac{2-\eta_{1c}}{\eta_{1c}} N_c$
$\square \eta_{1h}$	$2 \frac{1-\eta_{1h}}{\eta_{1h}\eta_{1c}} N_h$	$2 \frac{1-\eta_{1h}}{\eta_{1h}} N_h$
$\triangle G$	$\frac{1}{\eta_{1h}\eta_{1c}} N_{ex}$	$N_{ex}$
$\square \eta_2$	$\frac{1-\eta_2}{\eta_2 G \eta_{1h} \eta_{1c}} N_h$	$\frac{1-\eta_2}{\eta_2} N_h$
$\triangle G_H$	$\frac{1}{\eta_2 G \eta_{1h} \eta_{1c}} N_H$	$N_H$

with

$$N'_\Sigma = \frac{1 - \eta_{1c}}{\eta_{1c}} N_c + \frac{1 - \eta_{1h}}{\eta_{1h}\eta_{1c}} N_h + \frac{1 - \eta_2}{\eta_2 \eta_{1h} \eta_{1c}} N_h + \frac{1}{\eta_2 \eta_{1h} \eta_{1c}} N_H. \quad (\text{A10})$$

Varying  $N_{in}^s$ , we retrieve  $N'_\Sigma$ . Then, knowing the transmission efficiencies from the loss budget (see Appendix F), we can calculate  $N_H$ .

## 2. Noise rise

The noise-rise measurement consists of comparing the output noise power, recorded on the SA, when the KITWPA is on and off; knowing  $G$  and  $N'_\Sigma$ , we can retrieve  $N_\Sigma$ .

With the MS actuated toward the KITWPA, the HEMT-output noise obtained with the KITWPA off (pump off, no dc bias) is equal to that of Eq. (A9) (assuming that the loss between the two MS paths is equal and that signals from the DUT are transmitted with efficiency  $\eta_{1c}$  at 30 mK). But here,  $N_{in}^s = N_c$ , because there is vacuum noise at the signal input of the chain. Similarly, the HEMT-output noise obtained with the KITWPA on is equal to that of Eq. (A7), with  $N_{in}^s = N_c$ , such that the ratio of output noises  $r$  is

$$r = G \frac{N_\Sigma + N_c}{N'_\Sigma + N_c}, \quad (\text{A11})$$

which gives Eq. (2).

## APPENDIX B: EXCESS OF NOISE AND INTERNAL LOSS

The excess of noise in the KITWPA is associated with internal loss. Here, we evaluate this loss and show that it generates a noise commensurate with our observed excess noise of 1.9 K. We then discuss the possible origins of this loss.

### 1. From internal loss to transmission efficiency

Material loss can be characterized by the internal quality factor  $Q_i$  that a resonator fabricated in that material will have or, equivalently, by its loss tangent  $\tan \delta = 1/Q_i$ . In our case, we measure  $Q_i \simeq 5000$  on a Nb-Ti-N resonator at 4 K, the characteristics (line width, dc bias) of which are similar to those of the KITWPA.

In turn,  $Q_i$  can be expressed as a function of the field propagation constant  $\alpha + i\beta$  in that material, as  $Q_i = \beta/(2\alpha)$ . Here,  $\beta = k = \omega/v_p$  (excluding any dispersion engineering) where  $v_p$  is the phase velocity and  $\alpha$  is the (amplitude) attenuation constant. In our KITWPA,  $v_p = \lambda_s f_s \simeq 1000$  cells/ns, where  $\lambda_s$  is the wavelength of the periodic loading pattern that creates a stop band at frequency  $f_s$  [8]. Thus, with  $Q_i = 5000$  and at  $\omega = 2\pi \times 4.5$  GHz, we obtain  $\alpha \simeq 2.8 \times 10^{-6}$  cell $^{-1}$ .

Our KITWPA contains  $C_t = 66000$  cells; therefore, the total transmission efficiency is  $\eta_0 = \exp(-2\alpha C_t) \simeq 0.69$ . In other words, the total insertion loss in the KITWPA is equal to 1.6 dB. If we were to place this entire loss at the KITWPA signal and idler inputs, it would generate an excess noise  $T_{ex} = 3.6$  K for an effective gain  $G = 18$  dB. However, this loss is distributed along the line and that is why this naive calculation clearly overestimates the noise generated by this loss.

### 2. Excess noise from a distributed loss

The effect of distributed (and potentially asymmetric) loss on the ideal exponential gain of a traveling-wave parametric amplifier has been treated in theory [30,41]. Here, we distribute a known effective power gain  $G$  (that need not be perfectly exponential) and total transmission efficiency  $\eta_0$  within several stages, to evaluate the excess of noise associated with this distribution.

When the phase-matching condition is achieved in a traveling-wave parametric amplifier of length  $x$ , the output currents  $\tilde{A}(x)$  and  $\tilde{B}^*(x)$  at the signal and idler frequencies are [8,42]

$$\begin{aligned}\tilde{A}(x) &= A(x)e^{i2\chi k_a x}, \\ \tilde{B}^*(x) &= B^*(x)e^{i2\chi k_b x},\end{aligned}\quad (\text{B1})$$

where  $\chi$  is the cross-phase modulation term and  $k_a$  ( $k_b$ ) is the wave number at the signal (idler) frequency. The

amplitudes  $A(x)$  and  $B^*(x)$  are given by

$$\begin{pmatrix} A(x)/\sqrt{k_a} \\ B^*(x)/\sqrt{k_b} \end{pmatrix} = \begin{pmatrix} \cosh(g_3 x) & i \sinh(g_3 x) \\ -i \sinh(g_3 x) & \cosh(g_3 x) \end{pmatrix} \begin{pmatrix} A(0)/\sqrt{k_a} \\ B^*(0)/\sqrt{k_b} \end{pmatrix}. \quad (\text{B2})$$

In other words, for a given length of line  $x$ , the amplitude (i.e., gain) and phase of the currents are separately determined.

We now describe the signal and idler modes in terms of number operators. Their phase is determined by Eq. (B1). Then, for an amplifier with signal power gain  $G_0$ , preceded by a transmission efficiency  $\eta_0$  (modeled as a beam-splitter interaction), the amplitudes  $a_{in}$  and  $b_{in}$  of the input modes are transformed into the amplitudes  $a_{out}$  and  $b_{out}$  of the output modes according to

$$\begin{pmatrix} a_{out} \\ b_{out}^\dagger \end{pmatrix} = \begin{pmatrix} \sqrt{\eta_0 G_0} & i\sqrt{\eta_0(G_0 - 1)} \\ -i\sqrt{\eta_0(G_0 - 1)} & \sqrt{\eta_0 G_0} \end{pmatrix} \begin{pmatrix} a_{in} \\ b_{in}^\dagger \end{pmatrix}. \quad (\text{B3})$$

The effective signal gain power  $G$  (as observed on the VNA) is therefore equal to  $\eta_0 G_0$ . Considering now that the line has been divided into  $n$  identical stages (see Fig. 5), each characterized by a transmission efficiency  $\eta_n$  and gain  $G_n$ , the amplitude of the output modes is given by

$$\begin{pmatrix} a_{out} \\ b_{out}^\dagger \end{pmatrix} = \begin{pmatrix} \sqrt{\eta_n G_n} & i\sqrt{\eta_n(G_n - 1)} \\ -i\sqrt{\eta_n(G_n - 1)} & \sqrt{\eta_n G_n} \end{pmatrix}^n \begin{pmatrix} a_{in} \\ b_{in}^\dagger \end{pmatrix} = \begin{pmatrix} g_{aa}(n) & g_{ab}(n) \\ g_{ba}(n) & g_{bb}(n) \end{pmatrix} \begin{pmatrix} a_{in} \\ b_{in}^\dagger \end{pmatrix}, \quad (\text{B4})$$

where

$$g_{aa}(n) = \frac{1}{2} \left[ \left( \sqrt{\eta_n G_n} + \sqrt{\eta_n(G_n - 1)} \right)^n + \left( \sqrt{\eta_n G_n} - \sqrt{\eta_n(G_n - 1)} \right)^n \right] \quad (\text{B5})$$

and

$$g_{ab}(n) = -i \frac{1}{2} \left[ \left( \sqrt{\eta_n G_n} + \sqrt{\eta_n(G_n - 1)} \right)^n - \left( \sqrt{\eta_n G_n} - \sqrt{\eta_n(G_n - 1)} \right)^n \right], \quad (\text{B6})$$

and with  $g_{aa}(n) = g_{bb}(n)$  and  $g_{ab}(n) = -g_{ba}(n)$ . These relations define, for any number of stages  $n$ , the relation between  $\{\eta_n, G_n\}$  and  $\{\eta_0, G_0\}$ , because for any  $n$ , the overall values of the signal and idler amplitude gain are always equal to  $\sqrt{\eta_0 G_0}$  and  $i\sqrt{\eta_0(G_0 - 1)}$ , respectively. But we

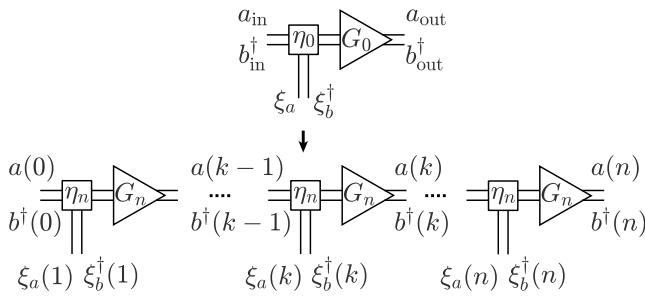


FIG. 5. A model for the distributed amplification and loss along the KITWPA. Starting with an amplifier with power gain  $G_0$  and a power transmission efficiency  $\eta_0$ , we divide the gain and loss along the KITWPA in  $n$  identical stages, each with transmission efficiency  $\eta_n$  and gain  $G_n$ .

can more easily calculate  $\eta_n$  and  $G_n$  in a recursive manner when  $n = 2^p$  where  $p \in \mathbb{N}$ , because then

$$\eta_{2^p} = \sqrt{\eta_{2^{p-1}}}, \quad (\text{B7})$$

$$G_{2^p} = \frac{\sqrt{G_{2^{p-1}}} + 1}{2}. \quad (\text{B8})$$

We now introduce the loss modes  $\xi_a(k)$  and  $\xi_b(k)$  for  $k \in \{1, n\}$  (see Fig. 5). These modes are complex, each with a random phase. The output of stage  $k$  is then given by

$$\begin{aligned} a(k) = & \sqrt{\eta_n G_n} a(k-1) + \sqrt{\eta_n (G_n - 1)} b^\dagger(k-1) \\ & + \sqrt{(1 - \eta_n) G_n} \xi_a(k) + \sqrt{(1 - \eta_n) (G_n - 1)} \xi_b^\dagger(k), \end{aligned} \quad (\text{B9})$$

$$\begin{aligned} b^\dagger(k) = & \sqrt{\eta_n (G_n - 1)} a(k-1) + \sqrt{\eta_n G_n} b^\dagger(k-1) \\ & + \sqrt{(1 - \eta_n) (G_n - 1)} \xi_a(k) + \sqrt{(1 - \eta_n) G_n} \xi_b^\dagger(k). \end{aligned} \quad (\text{B10})$$

Thus, we obtain recursively

$$\begin{aligned} a(n) = & g_{aa}(n) a(0) + g_{ab}(n) b^\dagger(0) \\ & + \sum_{j=1}^n \left[ c_a(j) \xi_a(j) + c_b(j) \xi_b^\dagger(j) \right], \end{aligned} \quad (\text{B11})$$

where, for  $j \in \{1, n\}$ ,

$$\begin{aligned} c_a(j) = & g_{aa}(n-j) \sqrt{(1 - \eta_n) G_n} \\ & + g_{ab}(n-j) \sqrt{(1 - \eta_n) (G_n - 1)} \end{aligned} \quad (\text{B12})$$

and

$$\begin{aligned} c_b(j) = & g_{aa}(n-j) \sqrt{(1 - \eta_n) (G_n - 1)} \\ & + g_{ab}(n-j) \sqrt{(1 - \eta_n) G_n}. \end{aligned} \quad (\text{B13})$$

We now need to calculate  $\langle a^\dagger(n) a(n) \rangle$ . Here, we assume that the loss modes are all uncorrelated and that they are all in equilibrium with a bath at temperature  $T_h$ , i.e.,  $\langle \xi_i^\dagger(k) \xi_j(l) \rangle = \delta_{ij} \delta_{kl} \bar{n}_h$ , where  $\bar{n}_h$  is the average photon number in each mode. We also assume that  $a(0)$  and  $b(0)$  are neither correlated to each other nor to any of the loss modes. With these conditions, we have

$$\begin{aligned} \langle a^\dagger(n) a(n) \rangle = & |g_{aa}(n)|^2 \left[ \langle a^\dagger(0) a(0) \rangle + \frac{1}{2} \right] + |g_{ab}(n)|^2 \left[ \langle b^\dagger(0) b(0) \rangle + \frac{1}{2} \right] \\ & + \sum_{j=1}^n |c_a(j)|^2 \left[ \langle \xi_a^\dagger(j) \xi_a(j) \rangle + \frac{1}{2} \right] + |c_b(j)|^2 \left[ \langle \xi_b^\dagger(j) \xi_b(j) \rangle + \frac{1}{2} \right] \\ & + \frac{1}{2} \left[ |g_{ab}(n)|^2 - |g_{aa}(n)|^2 + \sum_{j=1}^n |c_b(j)|^2 - |c_a(j)|^2 \right]. \end{aligned} \quad (\text{B14})$$

Finally, the last term of Eq. (B14) is equal to  $-1/2$  because  $|g_{ab}(n)|^2 - |g_{aa}(n)|^2 = -\eta_n^n$  and because  $|c_b(j)|^2 - |c_a(j)|^2 = (1 - \eta_n) \eta_n^j$ , for  $j \in \{1, n\}$ . We thus obtain

$$N_{\text{out}}^s = g_{aa}^2(n) N_{\text{in}}^s + g_{ab}^2(n) N_{\text{in}}^i + N_{\text{ex}}, \quad (\text{B15})$$

where

$$N_{\text{ex}} = N_h \sum_{j=1}^n [|c_a(j)|^2 + |c_b(j)|^2]. \quad (\text{B16})$$

Here,  $N_{\text{out}}^s = \langle a^\dagger(n) a(n) \rangle + 1/2$ ,  $N_{\text{in}}^s = \langle a^\dagger(0) a(0) \rangle + 1/2$ ,  $N_{\text{in}}^i = \langle b^\dagger(0) b(0) \rangle + 1/2$ , and  $N_h = \langle \xi_a^\dagger(j) \xi_a(j) \rangle + 1/2 =$

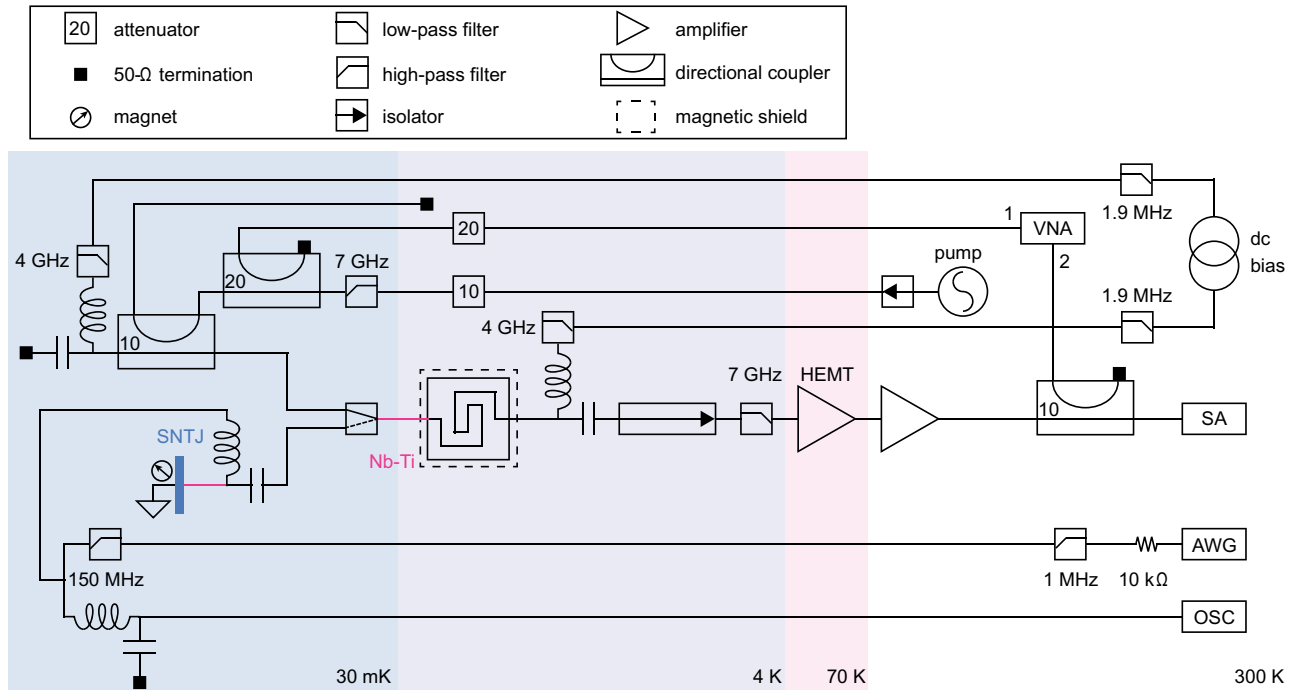


FIG. 6. The full experimental setup used to measure the noise performance of the KITWPA at 4 K.

$\langle \xi_b^\dagger(j) \xi_b(j) \rangle + 1/2$ , for  $j \in \{1, n\}$ . Equation (B15) is the equivalent of Eq. (1) when accounting for a distributed loss within the traveling-wave parametric amplifier.

In practice, the excess noise quickly converges to an asymptotic value, as we increase the number of divisions  $n$ , because gain and loss equilibrate. At  $n = 1024$ , it can be considered as asymptotic. Starting with  $\eta_0 = 0.69$  and  $G = 18$  dB, we thus estimate that  $T_{\text{ex}} = 0.5$  K. Therefore, this shows that the excess noise implied by the nonzero loss along the line is clearly non-negligible. The discrepancy between this theoretical value and the experimental one (1.9 K) may come from uncertainties in the true attenuation constant of the line (i.e.,  $Q_i$ ) but also from the possible inhomogeneous distribution of the loss, which may be greater at the beginning of the line.

### 3. Possible origin for the internal loss

Several phenomena can give rise to internal loss, including an excess of quasiparticles, two-level systems in the dielectric, or itinerant vortices. A recent study on a Nb-Ti-N transmission line embedded in an amorphous silicon matrix [11] suggests that itinerant vortices arise when dc biasing the line. Further study is required to identify and quantify the various possible sources of loss.

## APPENDIX C: FULL EXPERIMENTAL SETUP

### 1. Existing setup

The full experimental setup used to measure the chain-added noise containing the KITWPA is shown in

Fig. 6. It is composed of three main parts: the KITWPA control electronics (top), the amplification chain (middle), and the SNTJ control electronics (bottom). At the top, a current source and a microwave generator provide the dc and rf KITWPA biases, respectively. The high-pass filter on the pump line (ZHSS-8G-S+) provides over 30 dB of insertion loss at 6.5 GHz and over 80 dB at 4 GHz. In addition, a vector network analyzer (VNA) is connected to the input and output of the amplification chain, allowing us to measure the KITWPA gain.

In the middle, the amplification chain contains three amplifiers: the KITWPA at 4 K, the HEMT at 70 K, and a room-temperature amplifier (LNA-30-00101200-17-10P). Signals from the millikelvin stage, either vacuum noise or calibrated noise from the SNTJ, travel through these amplifiers and are read on the spectrum analyzer at room temperature.

Because of cable resistance between the SNTJ and its drive generator (the AWG), we cannot directly voltage bias the SNTJ. Instead, we current bias it with  $I_b$  (through a 10-kΩ polarization resistor) and retrieve  $V = R_{\text{SNTJ}}I_b$  by first measuring the SNTJ resistance  $R_{\text{SNTJ}}$ . To do that, we send a known dc current with the AWG and measure the dc voltage across the SNTJ with the oscilloscope (OSC), mounted in a four-point probe configuration (and set with the 1-MΩ input impedance).

### 2. Possible improvements

Ultimately, the BT and the DC presently placed at 30 mK and used to inject, respectively, the dc bias and rf

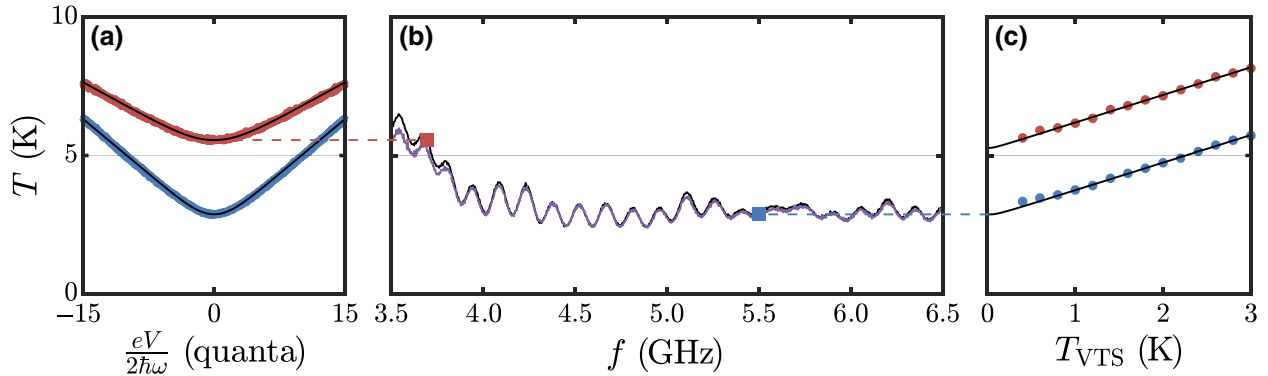


FIG. 7. The characterization of a HEMT-only amplifier chain (mounted at 4 K). (a) The output noise temperature is referred to the input of the chain (i.e., divided by the gain of the chain) and varies as a function of the SNTJ dc-bias voltage  $V$ . We illustrate the output noise recorded on the SA, in a 5-MHz window around two frequencies: 3.6 GHz (red curve) and 5.5 GHz (blue curve). We then retrieve the chain-added noise temperature  $T_{\Sigma 2}$  from a fit (black curves). (b) Two techniques allow us to measure  $T_{\Sigma 2}$  as a function of frequency: one using the shot noise generated by the dc-biased SNTJ (black curve) and one using the temperature-dependent Johnson noise generated by the unbiased SNTJ, mounted on a VTS (purple curve). Two squares underline the values of  $T_{\Sigma 2}$ : at 3.6 GHz, obtained with the shot-noise method (red); and at 5.5 GHz, obtained with the Johnson-noise method (blue). (c) The input-referred output noise temperature varies as a function of the VTS temperature. We illustrate this variation for two frequencies, 3.6 GHz (red points) and 5.5 GHz (blue points). We then recover  $T_{\Sigma 2}$  from a fit (black lines).

pump, should be made more compatible with the scarce real estate of the millikelvin stage. That means, ideally, placing them at 4 K. With off-the-shelf components, that would bring an additional 0.5–1.0 dB of insertion loss in front of the KITWPA, which would degrade the noise performance by a few kelvins: the chain-added noise would then be around 10 K. This noise may still be suitable for qubit readout, where a quantum-limited preamplifier is often placed at the millikelvin stage, typically a Josephson device, which routinely achieves 20–25 dB of gain [13,43]. This preamplifier would bring the 10-K chain-added noise below that of vacuum at the input of the chain. In the future, the BT and DC could be implemented on chip, together with the KITWPA, thereby reducing their insertion loss. Ultimately, this seems like a natural path forward. Note that any other traveling-wave parametric amplifier faces the same issue of pump delivery.

Note also that the (3.5–6.5)-GHz range over which the KITWPA has gain depends on the periodic loading inside the transmission line of the KITWPA, which determines the position of the pump frequency at which exponential gain is achieved [8]. This range can be adjusted by changing the design of the periodic loading (its period and impedance). As such, there is no fundamental obstacle to having the same technology operate in the (6–10)-GHz range, which is more favorable for qubit readout. Although dielectric loss will increase with frequency, so will the gain, for a fixed KITWPA length. Therefore, we do not expect the noise performance to be drastically different in the (6–10)-GHz range, compared with what is shown in the present work.

#### APPENDIX D: 4-K HEMT AMPLIFICATION CHAIN

We present in Fig. 8 an amplification chain where the 4-K HEMT is the first amplifier. Compared with that of Fig. 6, several components are removed from the signal path, notably the bias tees used to deliver the dc current  $I_d$  to the KITWPA and the low-pass filter that protects the HEMT from the strong KITWPA rf pump tone. We choose to keep the isolator because it is often placed before the HEMT in qubit experiments to avoid back action [44] and in satellite mission concepts [19,21] but we place it at millikelvin temperatures to minimize its noise contribution. The unavoidable SNTJ packaging and bias tee remain in the chain.

Generating shot noise with the dc-biased SNTJ and fitting the output noise recorded on the SA [see Fig. 7(a)], we obtain  $T_{\Sigma 2}$  as a function of frequency, shown in Fig. 7(b). To validate this result, we employ another, independent technique: in fact, at the input of the chain the SNTJ (with its packaging) is mounted on a variable temperature stage (VTS), allowing us to generate a temperature-dependent Johnson noise with the unbiased SNTJ. Fitting the output noise [see Fig. 7(c)], we obtain a second estimate of  $T_{\Sigma 2}$ . Here, the reference plane of the chain advances to the SNTJ packaging output, because the temperature of the packaging also varies. Then, comparing the gains of the chain between the two measurements (SNTJ and VTS), we estimate the SNTJ-packaging insertion loss to be  $0.3 \pm 0.3$  dB in the band of interest (see Appendix F), similar to previous evaluations [45]. The quantitative agreement

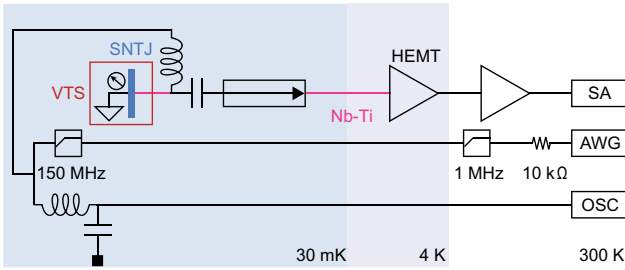


FIG. 8. An amplification chain where the HEMT is the first amplifier, placed at 4 K. The SNTJ and its packaging are mounted on a VTS.

between both methods validates our use of the SNTJ as a calibrated noise source.

## APPENDIX E: FIT OF NOISE CURVES

### 1. Shot-noise curves

We follow the same fitting procedure as in Ref. [8] but in the simpler case where we do not include the idler noise contribution. In short, the SNTJ delivers noise to the chain [8,43], the power of which is

$$N_{\text{in}}^s = \frac{k_B T}{2\hbar\omega_s} \left[ \frac{eV + \hbar\omega_s}{2k_B T} \coth\left(\frac{eV + \hbar\omega_s}{2k_B T}\right) + \frac{eV - \hbar\omega_s}{2k_B T} \coth\left(\frac{eV - \hbar\omega_s}{2k_B T}\right) \right], \quad (\text{E1})$$

where  $T$  is the SNTJ temperature,  $V$  is the voltage across the SNTJ, and  $\omega_s$  the signal frequency. The output noise recorded on the SA is proportional to that of Eq. (A9).

In practice, we first fit the output noise at high voltage  $V$ , for  $|eV/(2\hbar\omega_s)| > 3$  quanta. In that case, Eq. (E1) reduces to

$$N_{\text{in}}^s = \frac{eV}{2\hbar\omega_s}. \quad (\text{E2})$$

We obtain the gain  $G_c$  of the chain and the first estimation of  $N'_\Sigma$ .

Then we fit the central region, with  $G_c$  fixed. We let  $N'_\Sigma$  vary within  $\pm 25\%$  of its first estimation and because the AWG has a slight voltage offset  $V_{\text{off}}$ , we include it as a fit parameter: we write  $V - V_{\text{off}}$  instead of  $V$  in Eq. (E1). Finally, we bound  $T$  to a maximum value of 1 K.

### 2. Johnson-noise curves

When varying the VTS temperature, we deliver noise to the chain, the power of which is

$$N_{\text{in}}^s = \frac{1}{2} \coth\left(\frac{\hbar\omega}{2k_B T_{\text{VTS}}}\right). \quad (\text{E3})$$

TABLE IV. The transmission efficiencies at the various stages of the amplification chain and their subcomponents, averaged between 3.5 and 5.5 GHz. In addition to the ones defined in the text,  $\eta_{\alpha h}$  is the transmission of the cable at 4 K, before the KITWPA, and  $\eta_{\beta h}$  is the transmission of all the components between the KITWPA and the HEMT (see Fig. 6).

Transmission efficiency	Subcomponent
$\eta_{1c} = 0.8 \pm 0.1$	$\eta_{\text{SNTJ}} = 0.93 \pm 0.07$
$\eta_{1h} = 0.8 \pm 0.1$	$\eta_{\alpha c} = 0.86 \pm 0.05$
$\eta_2 = 0.51 \pm 0.1$	$\eta_{\alpha h} = 0.94 \pm 0.05$
	$\sqrt{\eta_p} = 0.85 \pm 0.1$
	$\sqrt{\eta_p} = 0.85 \pm 0.1$
	$\eta_{\beta h} = 0.6 \pm 0.05$

Knowing  $T_{\text{VTS}}$ , we fit the output noise recorded on the SA to obtain  $N_\Sigma = T_\Sigma k_B / (\hbar\omega)$ , the added noise of the chain containing only the HEMT at 4 K (see in Appendix D).

## APPENDIX F: LOSS BUDGET

We measure at 4 K the transmission of each part of the amplification chain with a VNA, to retrieve  $\eta_{1c}$ ,  $\eta_{1h}$  and  $\eta_2$  as a function of the frequency [see Fig. 9(a)]. To find  $\eta_{1c}$ , we first measure the transmission  $\eta_{\alpha c}$  of the chain from the output of the SNTJ packaging to the input of the Nb-Ti cable that connects the 30-mK stage to the 4-K stage. The SNTJ being a one-port device, we cannot measure the transmission of the SNTJ packaging  $\eta_{\text{SNTJ}}$  directly. Instead, we find it from the noise measurements performed on the chain solely containing the HEMT at 4 K:  $\eta_{\text{SNTJ}} = 0.93 \pm 0.07$  is the ratio between the gain of the chain obtained when using the SNTJ (proportional to  $G_H \eta_2 \eta_{1h} \eta_{\alpha c} \eta_{\text{SNTJ}}$ ) to the gain obtained when using the VTS (proportional to  $G_H \eta_2 \eta_{1h} \eta_{\alpha c}$ ). We then have  $\eta_{1c} = \eta_{\alpha c} \eta_{\text{SNTJ}}$ . The KITWPA packaging transmission  $\eta_p$  is measured separately at 4 K with a low probe tone power. It is then equally divided between  $\eta_{1h}$  and  $\eta_2$ . We report in Table IV the values of the various transmission efficiencies, along with their subcomponents.

Knowing all the transmission efficiencies, we use Eq. (A10) to deduce  $N_H$ , the HEMT-added noise at 70 K, from  $N'_\Sigma$ , the noise added by the chain presented in Fig. 1(b) (and measured with the SNTJ). In Fig. 9(b), we present  $T_H = N_H \hbar\omega / k_B$  as a function of the frequency, along with the manufacturer specifications for the HEMT-added noise, when the HEMT is at 4 K and 296 K [29]. Unsurprisingly,  $T_H$  lies between these two reported performances, with  $T_H = 10.7 \pm 0.4$  K between 3.5 and 5.5 GHz (uncertainty dominated by that of the transmission efficiencies).

Then, using Eq. (A8), we deduce  $N_{\text{ex}}$ , the KITWPA excess noise. In Fig. 9(c), we show  $T_{\text{ex}} = N_{\text{ex}} \hbar\omega / k_B$ , along with  $T_\Sigma$ , as a function of the frequency. In the (3.5–5.5)-GHz band, we have  $T_{\text{ex}} = 1.9 \pm 0.2$  K.

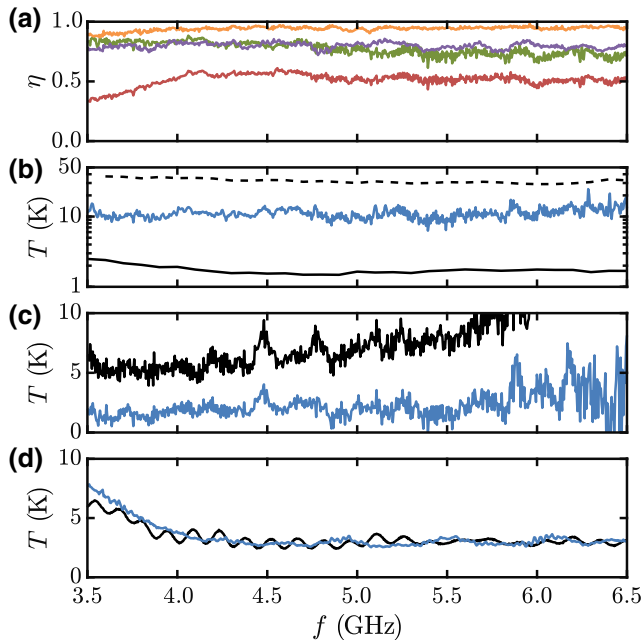


FIG. 9. The loss budget and the inferred noise temperatures. (a) The transmission efficiencies  $\eta_{1c}$  (purple line),  $\eta_{1h}$  (green), and  $\eta_2$  (red) are measured at 4 K. The SNTJ-packaging transmission  $\eta_{\text{SNTJ}}$  (orange line) is deduced from the ratio of gains of the chain, obtained when using the SNTJ and the VTS. (b) The HEMT-added noise temperature  $T_H$  (blue line) is then deduced using Eq. (A10). In comparison, we also show the noise temperature of the HEMT when it is at 4 K (solid black line) and 296 K (dashed black line). (c) The KITWPA excess noise temperature  $T_{\text{ex}}$  (blue line) is then calculated with Eq. (A8) using the data presented in (a) and (b) and using  $T_\Sigma$  (black line). (d) Both the measured (black line) and inferred (blue line) chain-added noise temperature  $T_\Sigma$  agree quantitatively well. The inference is made from the manufacturer specification of the HEMT-added noise at 4 K and from transmission-efficiency measurements on the parts of the chain shown in Fig. 8.

Finally, we also measure (at 4 K) the transmission efficiencies of each parts of the chain presented in Fig. 8, where the HEMT is mounted at 4 K. Then, from the manufacturer's specification of the HEMT-added noise at 4 K [see Fig. 9(b)], we calculate the expected chain-added noise and compared it with the measured one [see Fig. 9(d)]. Both are in good quantitative agreement, validating our overall methodology for the loss budget.

## APPENDIX G: FOUR-POINT PROBE SETUP

In Fig. 10, we present the experimental setup used to evaluate the dc power consumption of the KITWPA. With the KITWPA under dc and rf biases, we measure the voltage drop between components at 4 K required to operate the KITWPA, consisting of the KITWPA itself, the BT, and the LPF placed after the dc input of the BT. At room temperature, a voltmeter reads the voltage across these

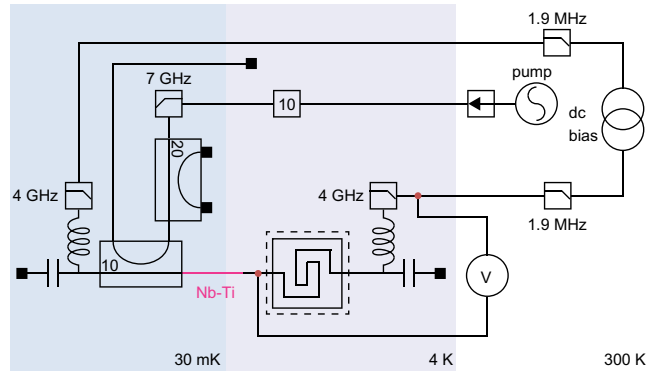


FIG. 10. The four-point probe experimental setup. Two red points highlight the ports across which we measure the voltage drop while the KITWPA is under dc and rf biases.

components. Note that we terminate the rf amplification chain at 4 K, because it is no longer properly matched to  $50 \Omega$ : in fact, we insert a subminiature version A (SMA) T-junction at the KITWPA input in order to read the potential at this point.

- [1] B. Yurke, L. R. Corruccini, P. G. Kaminsky, L. W. Rupp, A. D. Smith, A. H. Silver, R. W. Simon, and E. A. Whittaker, Observation of parametric amplification and deamplification in a Josephson parametric amplifier, *Phys. Rev. A* **39**, 2519 (1989).
- [2] M. A. Castellanos-Beltran, K. D. Irwin, G. C. Hilton, L. R. Vale, and K. W. Lehnert, Amplification and squeezing of quantum noise with a tunable Josephson metamaterial, *Nat. Phys.* **4**, 929 (2008).
- [3] N. Bergeal, F. Schackert, M. Metcalfe, R. Vijay, V. E. Manucharyan, L. Frunzio, D. E. Prober, R. J. Schoelkopf, S. M. Girvin, and M. H. Devoret, Phase-preserving amplification near the quantum limit with a Josephson ring modulator, *Nature* **465**, 64 (2010).
- [4] B. H. Eom, P. K. Day, H. G. LeDuc, and J. Zmuidzinas, A wideband, low-noise superconducting amplifier with high dynamic range, *Nat. Phys.* **8**, 623 (2012).
- [5] C. Macklin, K. O'Brien, D. Hover, M. E. Schwartz, V. Bolkhovsky, X. Zhang, W. D. Oliver, and I. Siddiqi, A near-quantum-limited Josephson traveling-wave parametric amplifier, *Science* **350**, 307 (2015).
- [6] N. E. Frattini, U. Vool, S. Shankar, A. Narla, K. M. Sliwa, and M. H. Devoret, 3-wave mixing Josephson dipole element, *Appl. Phys. Lett.* **110**, 222603 (2017).
- [7] L. Planat, A. Ranadive, R. Dassonneville, J. Puertas Martínez, S. Léger, C. Naud, O. Buisson, W. Hasch-Guichard, D. M. Basko, and N. Roch, Photonic-Crystal Josephson Traveling-Wave Parametric Amplifier, *Phys. Rev. X* **10**, 021021 (2020).
- [8] M. Malnou, M. R. Vissers, J. D. Wheeler, J. Aumentado, J. Hubmayr, J. N. Ullom, and J. Gao, Three-wave mixing kinetic inductance traveling-wave amplifier with near-quantum-limited noise performance, *PRX Quantum* **2**, 010302 (2021).

- [9] M. Malnou, D. A. Palken, L. R. Vale, G. C. Hilton, and K. W. Lehnert, Optimal Operation of a Josephson Parametric Amplifier for Vacuum Squeezing, *Phys. Rev. Appl.* **9**, 044023 (2018).
- [10] S. Chaudhuri, D. Li, K. D. Irwin, C. Bockstiegel, J. Hubmayr, J. N. Ullom, M. R. Vissers, and J. Gao, Broadband parametric amplifiers based on nonlinear kinetic inductance artificial transmission lines, *Appl. Phys. Lett.* **110**, 152601 (2017).
- [11] S. Shu, N. Klimovich, B. H. Eom, A. D. Beyer, R. Basu Thakur, H. G. Leduc, and P. K. Day, Nonlinearity and wide-band parametric amplification in a (Nb, Ti)N microstrip transmission line, *Phys. Rev. Res.* **3**, 023184 (2021).
- [12] D. J. Parker, M. Savitskyi, W. Vine, A. Laucht, T. Duty, A. Morello, A. L. Grimsom, and J. J. Pla, A near-ideal degenerate parametric amplifier, arXiv preprint [arXiv:2108.10471](https://arxiv.org/abs/2108.10471) (2021).
- [13] F. Arute *et al.*, Quantum supremacy using a programmable superconducting processor, *Nature* **574**, 505 (2019).
- [14] B. M. Brubaker, L. Zhong, Y. V. Gurevich, S. B. Cahn, S. K. Lamoreaux, M. Simanovskaja, J. R. Root, S. M. Lewis, S. Al Kenany, K. M. Backes, I. Urdinaran, N. M. Rapidis, T. M. Shokair, K. A. van Bibber, D. A. Palken, M. Malnou, W. F. Kindel, M. A. Anil, K. W. Lehnert, and G. Carosi, First Results from a Microwave Cavity Axion Search at 24  $\mu\text{eV}$ , *Phys. Rev. Lett.* **118**, 061302 (2017).
- [15] N. Du *et al.*, (ADMX Collaboration), Search for Invisible Axion Dark Matter with the Axion Dark Matter Experiment, *Phys. Rev. Lett.* **120**, 151301 (2018).
- [16] K. M. Backes *et al.*, A quantum enhanced search for dark matter axions, *Nature* **590**, 238 (2021).
- [17] B. Dober, D. T. Becker, D. A. Bennett, S. A. Bryan, S. M. Duff, J. D. Gard, J. P. Hays-Wehle, G. C. Hilton, J. Hubmayr, J. A. B. Mates, C. D. Reintsema, L. R. Vale, and J. N. Ullom, Microwave squid multiplexer demonstration for cosmic microwave background imagers, *Appl. Phys. Lett.* **111**, 243510 (2017).
- [18] C. R. H. McRae, H. Wang, J. Gao, M. R. Vissers, T. Brecht, A. Dunsworth, D. P. Pappas, and J. Mutus, Materials loss measurements using superconducting microwave resonators, *Rev. Sci. Instrum.* **91**, 091101 (2020).
- [19] S. R. Bandler, J. A. Chervenak, A. M. Datesman, A. M. Devasia, M. J. DiPirro, K. Sakai, S. J. Smith, T. R. Stevenson, W. Yoon, D. A. Bennett, B. Mates, D. S. Swetz, J. N. Ullom, K. D. Irwin, M. E. Eckart, E. Figueroa-Feliciano, D. McCommon, K. K. Ryu, J. R. Olson, and B. Zeiger, Lynx x-ray microcalorimeter, *J. Astron. Telesc. Instrum. Syst.* **5**, 1 (2019).
- [20] M. DiPirro, S. Bandler, X. Li, J. Olson, J. Tuttle, W. Yoon, and M. Zagarola, Lynx x-ray microcalorimeter cryogenic system, *J. Astron. Telesc. Instrum. Syst.* **5**, 1 (2019).
- [21] P. M. Echternach, A. D. Beyer, and C. M. Bradford, Large array of low-frequency readout quantum capacitance detectors, *J. Astron. Telesc. Instrum. Syst.* **7**, 1 (2021).
- [22] D. C. Bradley, T. L. Jamison-Hooks, J. G. Staguhn, E. G. Amatucci, T. Browning, M. J. DiPirro, D. T. Leisawitz, and R. C. Carter, On the advancements of digital signal processing hardware and algorithms enabling the Origins Space Telescope, *J. Astron. Telesc. Instrum. Syst.* **7**, 1 (2021).
- [23] M. C. Wiedner *et al.*, The Origins Space Telescope Mission Concept Study Team, Heterodyne receiver for Origins, *J. Astron. Telesc. Instrum. Syst.* **7**, 1 (2021).
- [24] NASA, “2020 decadal survey planning” (2021).
- [25] N. Zobrist, B. H. Eom, P. Day, B. A. Mazin, S. R. Meeker, B. Bumble, H. G. LeDuc, G. Coiffard, P. Szypryt, N. Fruitwala, I. Lipartito, and C. Bockstiegel, Wide-band parametric amplifier readout and resolution of optical microwave kinetic inductance detectors, *Appl. Phys. Lett.* **115**, 042601 (2019).
- [26] M. R. Vissers, R. P. Erickson, H.-S. Ku, L. Vale, X. Wu, G. C. Hilton, and D. P. Pappas, Low-noise kinetic inductance traveling-wave amplifier using three-wave mixing, *Appl. Phys. Lett.* **108**, 012601 (2016).
- [27] J. Zmuidzinas, Superconducting microresonators: Physics and applications, *Annu. Rev. Condens. Matter Phys.* **3**, 169 (2012).
- [28] L. Ranzani, M. Bal, K. C. Fong, G. Ribeill, X. Wu, J. Long, H.-S. Ku, R. P. Erickson, D. Pappas, and T. A. Ohki, Kinetic inductance traveling-wave amplifiers for multiplexed qubit readout, *Appl. Phys. Lett.* **113**, 242602 (2018).
- [29] [https://www.lownoisefactory.com/datasheets/LNF-LNC4\\_8C\\_sn1315H.pdf](https://www.lownoisefactory.com/datasheets/LNF-LNC4_8C_sn1315H.pdf).
- [30] C. M. Caves, Quantum limits on noise in linear amplifiers, *Phys. Rev. D* **26**, 1817 (1982).
- [31] J. M. Epstein, K. B. Whaley, and J. Combes, Quantum limits on noise for a class of nonlinear amplifiers, *Phys. Rev. A* **103**, 052415 (2021).
- [32] Y. Yamamoto and K. Inoue, Noise in amplifiers, *J. Lightwave Technol.* **21**, 2895 (2003).
- [33] L. Spietz, R. J. Schoelkopf, and P. Pari, Shot noise thermometry down to 10 mK, *Appl. Phys. Lett.* **89**, 183123 (2006).
- [34] P. Szypryt, S. R. Meeker, G. Coiffard, N. Fruitwala, B. Bumble, G. Ulbricht, A. B. Walter, M. Daal, C. Bockstiegel, G. Collura, N. Zobrist, I. Lipartito, and B. A. Mazin, Large-format platinum silicide microwave kinetic inductance detectors for optical to near-IR astronomy, *Opt. Express* **25**, 25894 (2017).
- [35] K. D. Irwin and K. W. Lehnert, Microwave squid multiplexer, *Appl. Phys. Lett.* **85**, 2107 (2004).
- [36] J. A. B. Mates, D. T. Becker, D. A. Bennett, B. J. Dober, J. D. Gard, J. P. Hays-Wehle, J. W. Fowler, G. C. Hilton, C. D. Reintsema, D. R. Schmidt, D. S. Swetz, L. R. Vale, and J. N. Ullom, Simultaneous readout of 128 x-ray and gamma-ray transition-edge microcalorimeters using microwave squid multiplexing, *Appl. Phys. Lett.* **111**, 062601 (2017).
- [37] L. Spietz, K. W. Lehnert, I. Siddiqi, and R. J. Schoelkopf, Primary electronic thermometry using the shot noise of a tunnel junction, *Science* **300**, 1929 (2003).
- [38] E. Cha, N. Wade Falk, G. Moschetti, A. Pourkabirian, J. Stenarson, and J. Grahn, in *2020 IEEE/MTT-S International Microwave Symposium (IMS)* (2020), p. 1299.
- [39] J. Bockstiegel, C. Gao, M. R. Vissers, M. Sandberg, S. Chaudhuri, A. Sanders, L. R. Vale, K. D. Irwin, and D. P. Pappas, Development of a broadband NbTiN traveling wave parametric amplifier for mkid readout, *J. Low Temp. Phys.* **176**, 476 (2014).

- [40] A. Ranadive, M. Esposito, L. Planat, E. Bonet, C. Naud, O. Buisson, W. Guichard, and N. Roch, A reversed Kerr traveling wave parametric amplifier, arXiv preprint [arXiv:2101.05815](https://arxiv.org/abs/2101.05815) (2021).
- [41] M. Houde, L. C. G. Govia, and A. A. Clerk, Loss Asymmetries in Quantum Traveling-Wave Parametric Amplifiers, *Phys. Rev. Appl.* **12**, 034054 (2019).
- [42] R. W. Boyd, *Nonlinear Optics* (Academic Press, London, 2019).
- [43] F. Lecocq, L. Ranzani, G. A. Peterson, K. Cicak, R. W. Simmonds, J. D. Teufel, and J. Aumentado, Nonreciprocal Microwave Signal Processing with a Field-Programmable Josephson Amplifier, *Phys. Rev. Appl.* **7**, 024028 (2017).
- [44] E. I. Rosenthal, C. M. F. Schneider, M. Malnou, Z. Zhao, F. Leditzky, B. J. Chapman, W. Wustmann, X. Ma, D. A. Palken, M. F. Zanner, L. R. Vale, G. C. Hilton, J. Gao, G. Smith, G. Kirchmair, and K. W. Lehnert, Efficient and Low-Backaction Quantum Measurement Using a Chip-Scale Detector, *Phys. Rev. Lett.* **126**, 090503 (2021).
- [45] S.-W. Chang, J. Aumentado, W.-T. Wong, and J. C. Bardin, in *2016 IEEE MTT-S International Microwave Symposium (IMS)* (IEEE, 2016), p. 1.